

## Supporting Information

### **Tert-butyl hydroperoxide-Mediated Rapid 30-Second Oxidation of 5-Hydroxymethylfurfural to 2,5-Furandicarboxylic Acid**

Jian Liu<sup>1,2</sup>, Ximing Zhang<sup>1,2\*</sup>

*1. State Key Laboratory (SKL) of Biobased Transportation Fuel Technology, College of  
Biosystems Engineering and Food Science, Zhejiang University, Hangzhou, 310058, China.*

*2. Institute of Zhejiang University-Quzhou, 99 Zheda Road, Quzhou, Zhejiang Province,  
324000, China*

\*Corresponding author:

Ximing Zhang, email address: [zhangximing@zju.edu.cn](mailto:zhangximing@zju.edu.cn).

## **Contents**

1. Literature survey of HMF selective oxidation to FDCA
2. Characterization of Au/CeO<sub>2</sub> catalyst
3. Catalytic data of Au/CeO<sub>2</sub> with TBHP for HMF selective oxidation to FDCA
4. Recycle tests of the Au/CeO<sub>2</sub> with TBHP for HMF selective oxidation to FDCA
5. TBHP and H<sub>2</sub>O<sub>2</sub> activation for Au/CeO<sub>2</sub>
6. Hydrophobic Interactions during TBHP mediated selective oxidation of HMF to FDCA

## Results and Discussion

### 1. Literature survey of HMF oxidation to FDCA

**Table S1.** Oxidation of HMF to FDCA over Au/CeO<sub>2</sub> catalyst.

catalyst	Solvent	T (°C)	t	Oxidant	molar ratio of HMF/Au	Conv. (%)	FDCA Yield (%)	Prod. (mmol*g <sub>Au</sub> <sup>-1</sup> h <sup>-1</sup> )	Ref.
Au/CeO <sub>2</sub>	0.4 m NaOH	90	30 s	0.4 mmol TBHP	100.00	100.0	95	57868.02	This work
Au/CeO <sub>2</sub>	2 m Na <sub>2</sub> CO <sub>3</sub>	140	15	0.5 MPa O <sub>2</sub>	78.00	99.0	95	25.08	1
Au/CeO <sub>2</sub> -rod	0.1 m NaOH	130	2.5	0.5 MPa O <sub>2</sub>	400.00	100.0	87	709.85	2
Au/CeO <sub>2</sub>	0.16 m NaOH	70	4	1 MPa O <sub>2</sub>	100.00	100.0	63	79.95	3
Au/CeO <sub>2</sub>	6×10 <sup>-5</sup> m NaOH	120	24	1.5 MPa O <sub>2</sub>	70.61	99.9	96	14.28	4
Au/CeO <sub>2</sub>	6×10 <sup>-5</sup> m NaOH	120	25	1.5 MPa O <sub>2</sub>	64.59	99.9	64	8.33	4
Au/CeO <sub>2</sub>	6×10 <sup>-5</sup> m NaOH	120	26	1.5 MPa O <sub>2</sub>	60.06	99.9	46	5.39	4

**Table S2.** Oxidation of HMF to FDCA over THBP oxidant.

catalyst	Solvent	T (°C)	t	Conv. (%)	FDCA		Ref.
					Yield (%)	Prod. (mmol*g <sub>cat</sub> <sup>-1</sup> *h <sup>-1</sup> )	
Au/CeO <sub>2</sub>	H <sub>2</sub> O, 0.4 m NaOH	90 <sup>a</sup>	30 s	100	95	568.38	this work
Au/CeO <sub>2</sub>	H <sub>2</sub> O, base-free	90 <sup>a</sup>	30 s	8	0	0	this work
M-resin-Co-Py	CH <sub>3</sub> CN, base-free	100 <sup>b</sup>	24 h	96	90	0.42	5
MIL-100(Fe)	H <sub>2</sub> O, base-free	70 <sup>b</sup>	24 h	100	57	0.94	6
Fe(NO <sub>3</sub> ) <sub>3</sub>	CH <sub>2</sub> Cl <sub>2</sub> , 0.03 equiv. NaCl	25 <sup>b</sup>	4 h	100	92	1.15	7
Nb-Si-1	CH <sub>3</sub> CN, base-free	140 <sup>b</sup>	48 h	97	62	0.21	8
MnCo <sub>2</sub> /NS-MS	CH <sub>3</sub> CN, base-free	120 <sup>b</sup>	12 h	100	72	1.67	9
Cu-MnO <sub>2</sub> NR	tert-butanol, base-free	80 <sup>b</sup>	12 h	100	96	0.42	10
Cu-MnO <sub>2</sub> @PDVTA	tert-butanol, base-free	80 <sup>b</sup>	24 h	100	97	2.08	11
CuMn <sub>2</sub> O <sub>4</sub>	CH <sub>3</sub> CN, base-free	80 <sup>b</sup>	12 h	100	96	4.00	12
Mn <sub>8</sub> Fe <sub>3</sub> Ox	DMSO, base-free	70 <sup>b</sup>	24 h	100	77	1.93	13
MnFe <sub>2</sub> O <sub>4</sub>	CH <sub>3</sub> CN, base-free	100 <sup>b</sup>	6 h	100	85	0.47	14
Fe <sub>3</sub> O <sub>4</sub> -CoOx	DMSO, base-free	80 <sup>b</sup>	12 h	97	69	0.32	15
10Co@22Nb@MNP	CH <sub>3</sub> CN, base-free	100 <sup>b</sup>	12 h	97	94	0.67	16

a: Microwave heating

b: Conventional heating

**Table S3.** Changes in Au Content of Au/CeO<sub>2</sub> and FDCA Yield Over Five Cycles.

Cycle	1	2	3	4	5
Au content (%)	0.97	0.44	0.19	0.16	0.13
FDCA yield (%)	94.73	9.62	2.73	1.94	1.16

Reaction conditions: HMF, 0.1 mmol; HMF/metal/TBHP molar ratio, 1:0.01:4; and H<sub>2</sub>O, 5 mL. The reaction time is 30 s. The reaction temperature is 90 °C.

## 2. Characterization of Au/CeO<sub>2</sub> catalyst

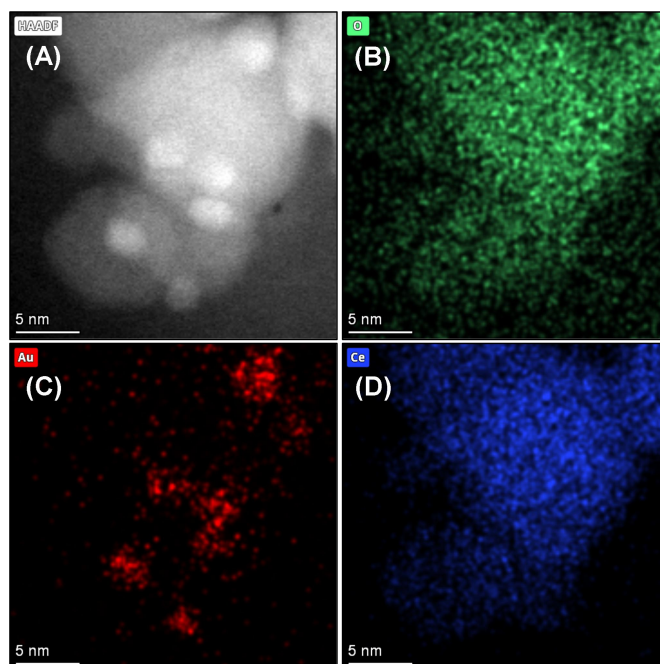


**Fig. S1.** EDS elemental maps of the Au/CeO<sub>2</sub> catalyst for O (A), Au (B) and Ce (C).

Note : The synthesized Au/CeO<sub>2</sub> catalyst was characterized by TEM with EDS, confirming the morphology, dispersion of Au nanoparticles, and homogeneous distribution of O, Au, and Ce across the CeO<sub>2</sub> support.

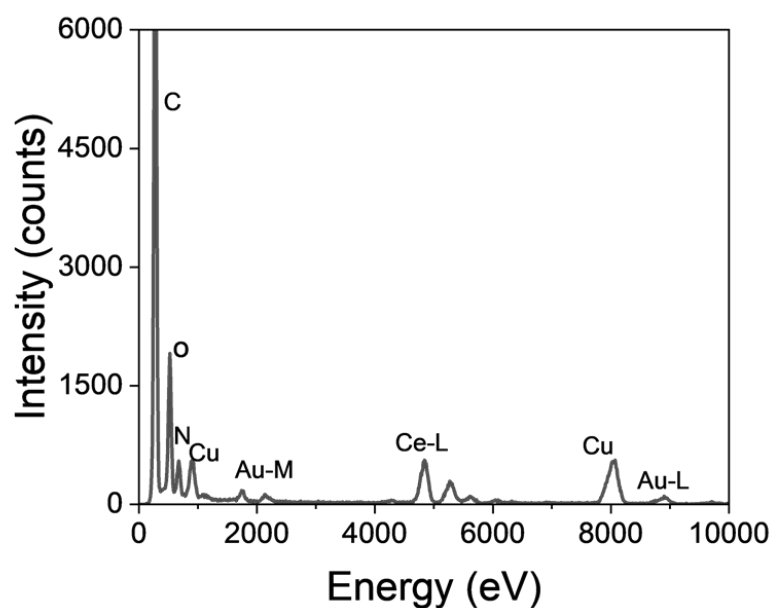


**Fig. S2.** EDS spectrum of Au/CeO<sub>2</sub>.

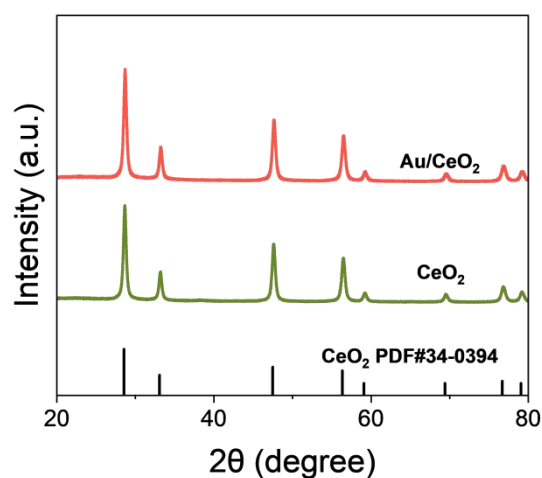


**Fig. S3.** XRD patterns of CeO<sub>2</sub>, the fresh Au/CeO<sub>2</sub> and the powder diffraction file of fluorite-type CeO<sub>2</sub> (PDF#34-0394).

Note: The structural of the synthesized Au/CeO<sub>2</sub> catalyst was investigated using X-ray diffraction (XRD). The XRD pattern of the fresh Au/CeO<sub>2</sub> catalyst exhibits characteristic peaks at 2θ values of 29.4°, 33.1°, 47.5°, and 56.4°, which correspond

to the (111), (200), (220), and (311) planes of the face-centered cubic phase of CeO<sub>2</sub> (JCPDS Card No. 34-0394). The absence of distinct peaks for metallic gold suggests that the gold nanoparticles are well dispersed on the CeO<sub>2</sub> support or are present in a highly dispersed state below the detection limit of XRD.

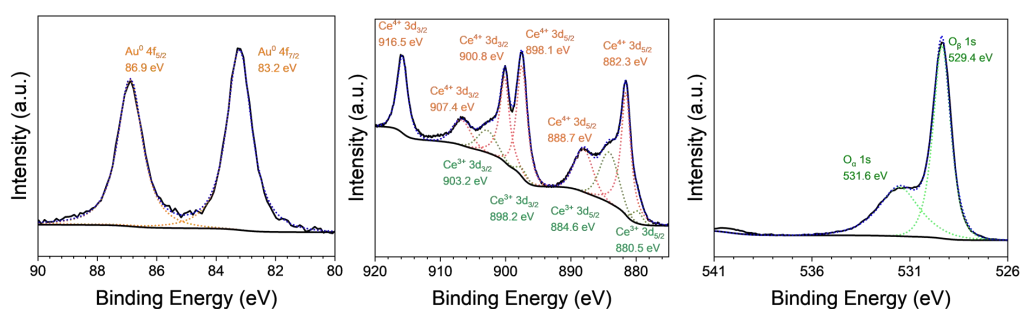


**Fig. S4.** XPS spectrum of the Au 4f, Ce 3d and O 1s region of Au/CeO<sub>2</sub>. The black line indicates the original spectrum; the green and orange broken lines indicate the deconvoluted signals, and the blue broken line indicates the sum of the deconvoluted signals.

Note: The XPS analysis provides further insights into the surface composition and oxidation states of the elements in the Au/CeO<sub>2</sub> catalyst. The Au 4f XPS spectrum (Fig. 1d) displays a spin-orbit doublet with binding energies at 83.9 eV and 87.6 eV, characteristic of metallic gold (Au<sup>0</sup>), indicating the presence of gold in its zero oxidation state on the catalyst surface. The Ce 3d XPS spectrum (Fig. 1e) is deconvoluted into several peaks corresponding to different oxidation states of cerium. The peaks at 882.3 eV and 898.1 eV are attributed to the Ce 3d<sub>5/2</sub> and Ce 3d<sub>3/2</sub> levels of Ce<sup>4+</sup>, while the peaks at 884.6 eV and 900.8 eV are associated with Ce<sup>3+</sup>, suggesting the presence of both Ce(IV) and Ce(III) on the catalyst surface.<sup>17</sup> This

coexistence of  $\text{Ce}^{4+}$  and  $\text{Ce}^{3+}$  is indicative of the redox properties of  $\text{CeO}_2$ , which is crucial for its catalytic performance. The O 1s XPS spectrum (Fig. 1f) shows a peak at 531.6 eV, which can be assigned to lattice oxygen in  $\text{CeO}_2$ , and a higher binding energy shoulder at 533.1 eV, which may be attributed to adsorbed oxygen species or surface hydroxyl groups.<sup>18, 19</sup> These surface oxygen species are believed to play a vital role in the catalytic oxidation process.

### 3. Catalytic data of Au/ $\text{CeO}_2$ with TBHP for HMF selective oxidation

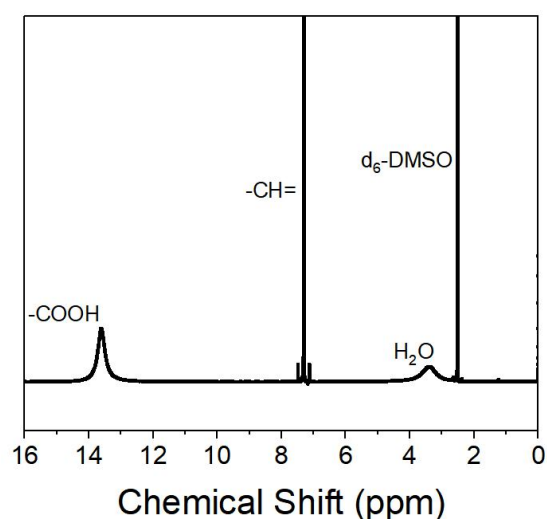


**Fig. S5.** <sup>1</sup>H NMR spectrum of the production after HMF oxidation with Au/ $\text{CeO}_2$ .

Note: NMR identified the product's characteristic features that are typical of FDCA.<sup>20</sup>

This finding, in conjunction with the product's retention time in HPLC matching that of the standard, confirmed that the product derived from HMF is FDCA.

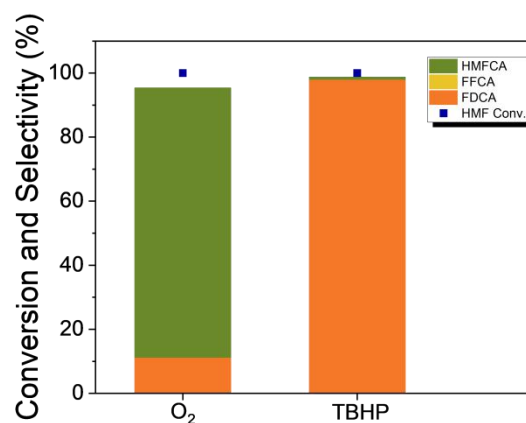


**Fig. S6.** Catalytic data characterizing the oxidation of HMF to FDCA over various oxidant in the high-pressure reactor. Reaction conditions: HMF, 0.1 mmol; HMF/metal/NaOH/TBHP molar ratio, 1:0.01:20:4; H<sub>2</sub>O, 5 mL. In reactions where O<sub>2</sub> serves as the oxidant, TBHP was not introduced, and the O<sub>2</sub> pressure was maintained at 1 MPa. The heating time is 25min. The reaction time is 30 s. The reaction temperature is 90 °C.

#### 4. Recycle tests of the Au/CeO<sub>2</sub> for HMF selective oxidation

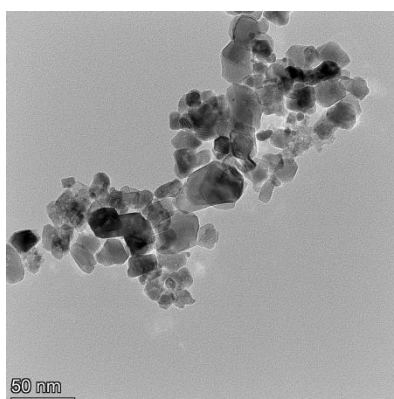


**Fig. S7.** TEM image of Au/CeO<sub>2</sub> used once.

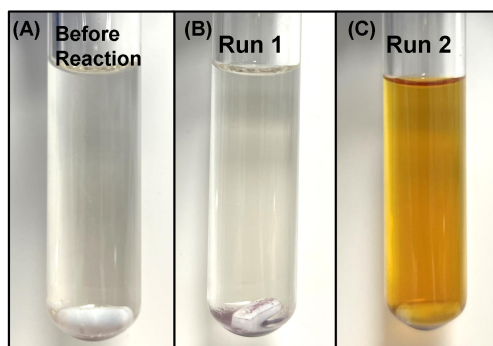


**Fig. S8.** Recycle tests of the Au/CeO<sub>2</sub> for HMF selective oxidation in 20 equiv NaOH to HMF. (A) Newly prepared reaction solution. (B) The reaction solution of the first cycle. (C) The reaction solution of the second cycle. Reaction conditions: HMF, 0.1 mmol; HMF/metal/TBHP molar ratio, 1:0.01:4; and H<sub>2</sub>O, 5 mL. The reaction time is 30 s. The reaction temperature is 90 °C.

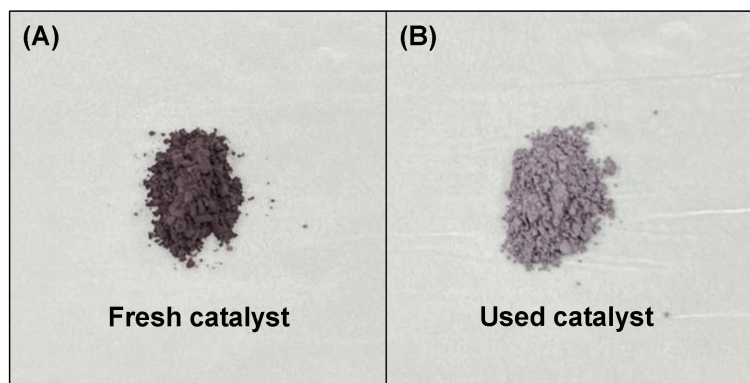


**Fig. S9.** Recycle tests of the Au/CeO<sub>2</sub> for HMF selective oxidation in 20 equiv NaOH to HMF. (A) Newly prepared Au/CeO<sub>2</sub> catalyst, (B) Au/CeO<sub>2</sub> catalyst used once. Reaction conditions: HMF, 0.1 mmol; HMF/metal/NaOH/TBHP molar ratio, 1:0.01:20:4; H<sub>2</sub>O, 5 mL. The reaction time is 30 s. The reaction temperature is 90 °C.

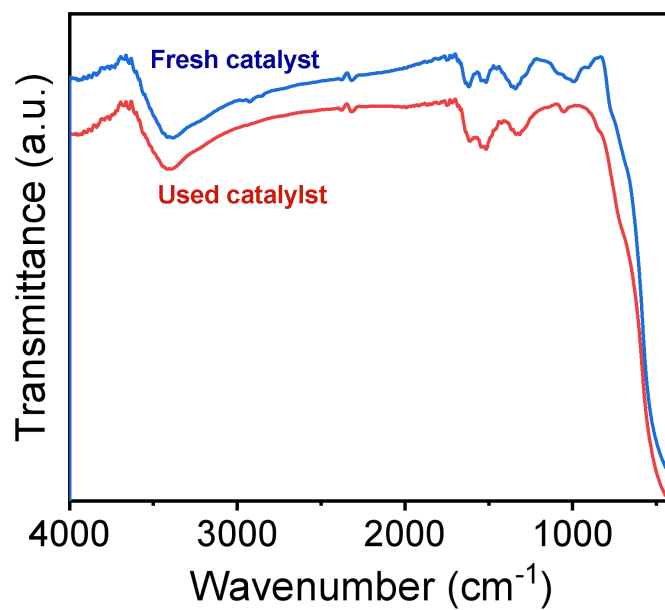


**Fig. S10.** FTIR spectra of the Fresh and used Au/CeO<sub>2</sub> catalyst.

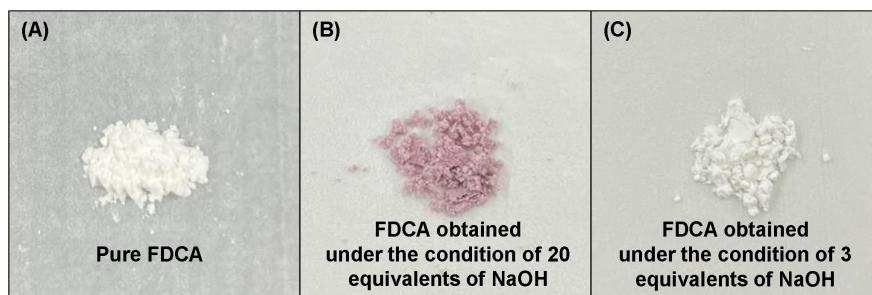


**Fig. S11.** Recycle tests of the Au/CeO<sub>2</sub> for HMF selective oxidation with different amount of base (A-G). Reaction conditions: HMF, 0.1 mmol; HMF/metal/NaOH/TBHP molar ratio, 1:0.01:20:4; H<sub>2</sub>O, 5 mL. The reaction time is 30 s. The reaction temperature is 90 °C.

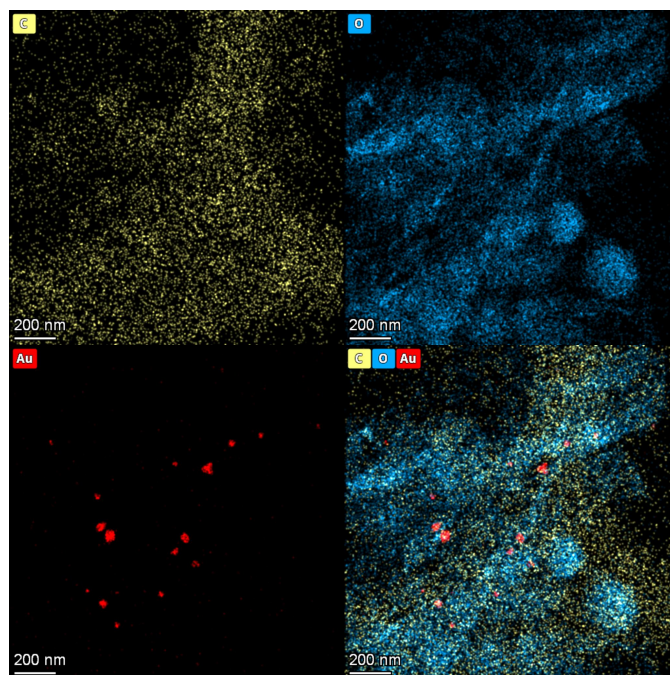


**Fig. S12.** EDS elemental mapping images for C, O and Au (Ce not detected) of the HMF oxidation production.

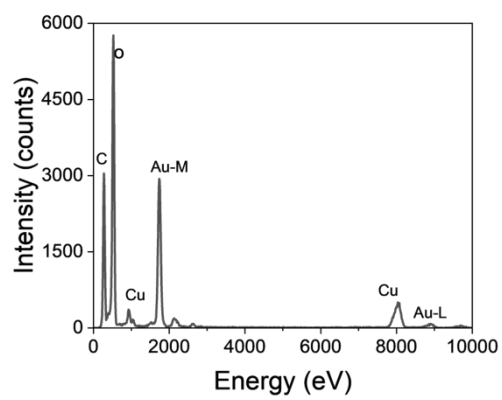


**Fig. S13.** EDS spectrum of HMF oxidation production.

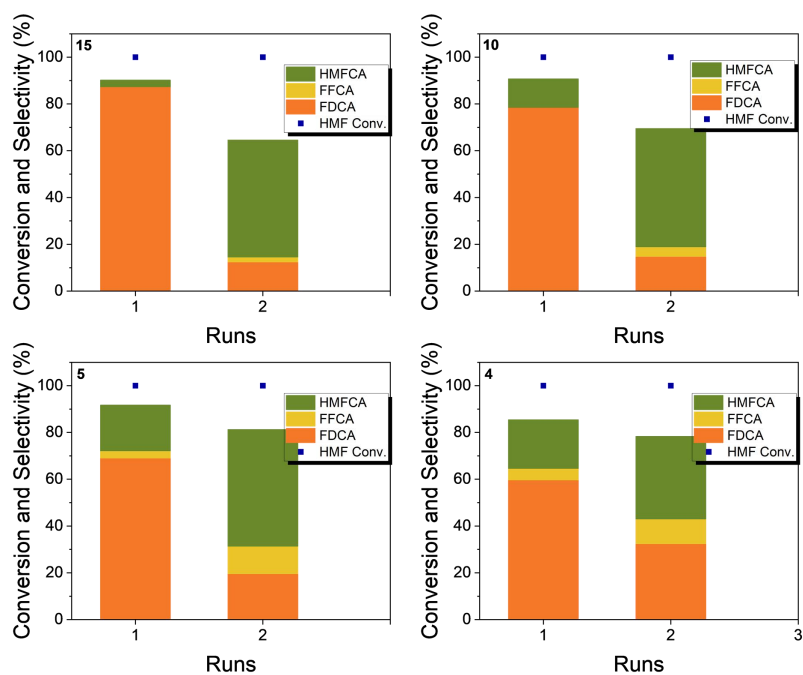


**Fig. S14.** Recycle tests of the Au/CeO<sub>2</sub> for HMF selective oxidation with different amount of base (A-G). Reaction conditions: HMF, 0.1 mmol; HMF/metal/TBHP molar ratio, 1:0.01:4; H<sub>2</sub>O, 5 mL. The reaction time is 30 s.

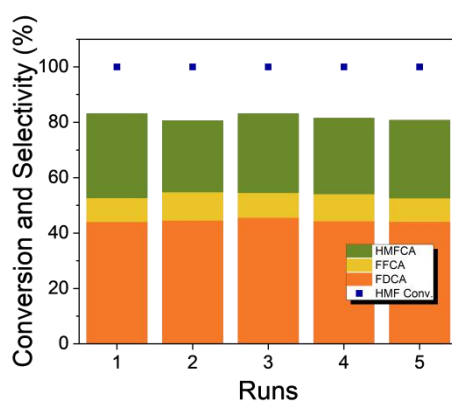


**Fig. S15.** Recycle tests of the Au/CeO<sub>2</sub> for HMF selective oxidation in 3 equiv NaOH to HMF (A-G). Reaction conditions: HMF, 0.1 mmol; HMF/metal/TBHP molar ratio, 1:0.01:4; H<sub>2</sub>O, 5 mL. The reaction time is 30 s. The reaction temperature is 90 °C.

## 5. TBHP and H<sub>2</sub>O<sub>2</sub> activation for Au/CeO<sub>2</sub>

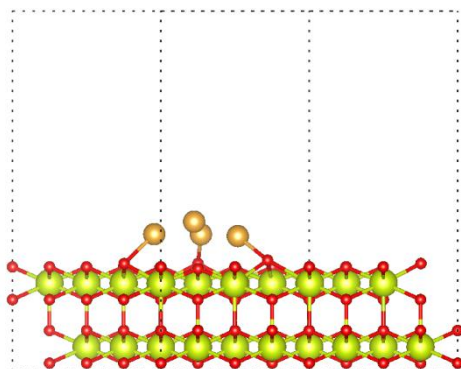


**Fig. S16.** The structural illustration for Au/CeO<sub>2</sub> (green, yellow, and red spheres represent Ce, Au and O, respectively).

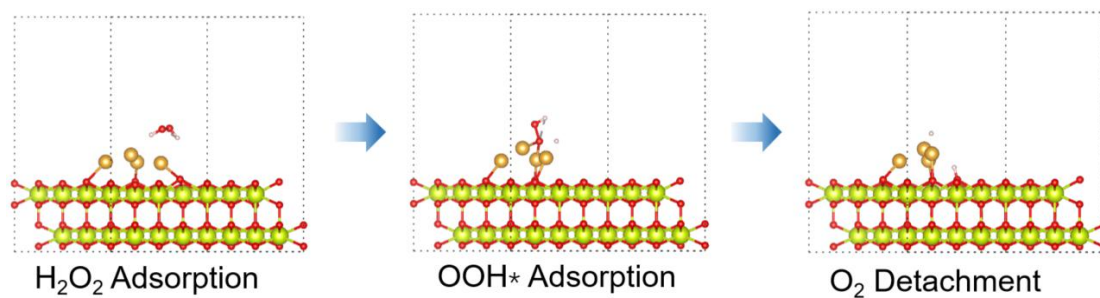


**Fig. S17.** H<sub>2</sub>O<sub>2</sub> activation process for Au/CeO<sub>2</sub> (green, yellow and, red, and white spheres represent Ce, Au, O, and H, respectively).

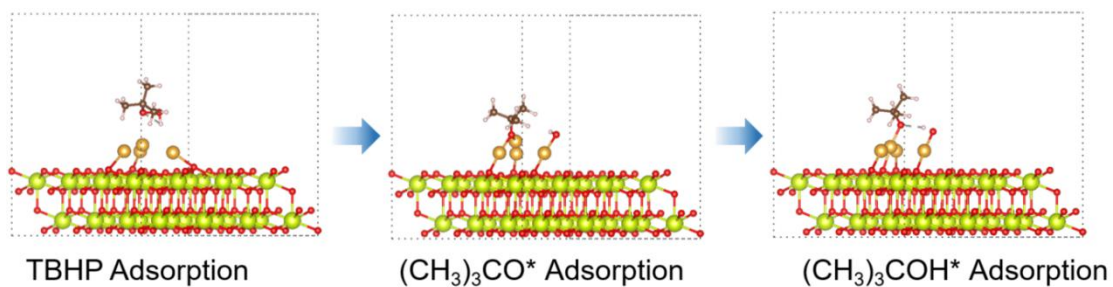


**Fig. S18.** TBHP activation process for Au/CeO<sub>2</sub> (green, yellow, red, white, and brown spheres represent Ce, Au, O, H, and C, respectively).

## 6. Hydrophobic Interactions during TBHP mediated selective oxidation of HMF to FDCA

**Table S4.**  $I_1$ ,  $I_3$  and  $I_1/I_3$  of Steady-state fluorescence emission spectra of pyrene for various control experiments.

	$I_1$ (373 nm)	$I_3$ (384 nm)	$I_1/I_3$
H <sub>2</sub> O	62999.30	77631.66	0.81
HMF+H <sub>2</sub> O	30051.09	56083.63	0.54
TBHP+H <sub>2</sub> O	46822.97	93982.73	0.50
HMF+TBHP+H <sub>2</sub> O	22731.60	59940.38	0.38

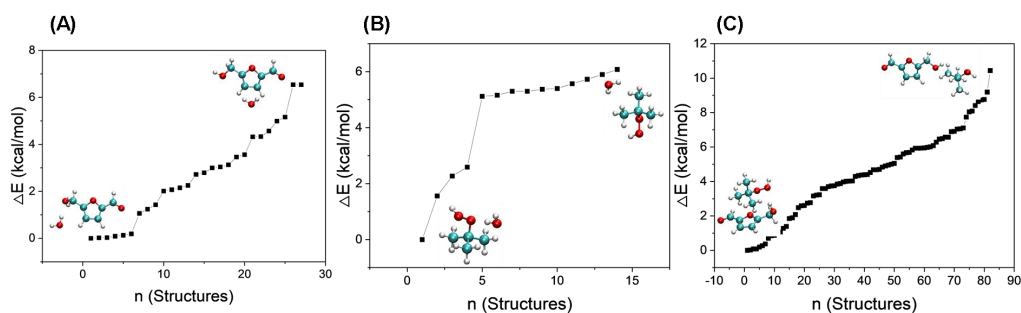


**Fig. S19.** Calculation of interaction energies for HMF-H<sub>2</sub>O (A), TBHP-H<sub>2</sub>O (B), and HMF-TBHP (C).

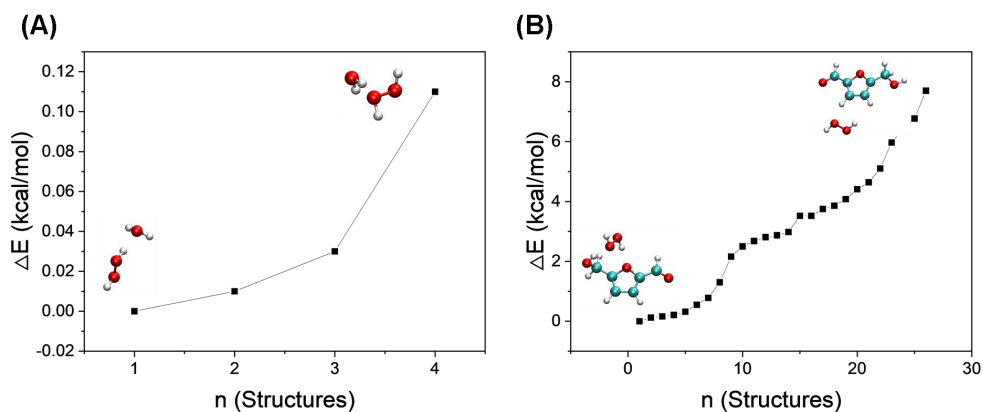
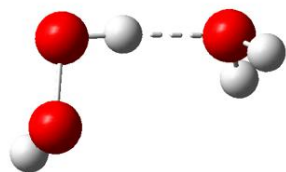
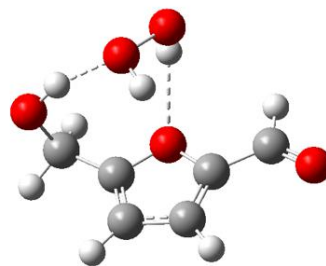


**Fig. S20.** Calculation process of interaction energies for H<sub>2</sub>O<sub>2</sub>-H<sub>2</sub>O, and HMF-H<sub>2</sub>O<sub>2</sub>.



$$\Delta E = -6.34 \text{ kcal/mol}$$



$$\Delta E = -7.79 \text{ kcal/mol}$$

**Fig. S21.** DFT calculated the interaction energy diagrams of HMF and H<sub>2</sub>O<sub>2</sub> in aqueous phase.

## References:

1. M. Kim, Y. Su, A. Fukuoka, E. J. Hensen and K. Nakajima, *Angewandte Chemie International Edition*, 2018, **57**, 8235-8239.
2. H. Xu, X. Li, W. Hu, Z. Yu, H. Zhou, Y. Zhu, L. Lu and C. Si, *ChemSusChem*, 2022, **15**, e202200352.
3. C. Megías-Sayago, K. Chakarova, A. Penkova, A. Lolli, S. Ivanova, S. Albonetti, F. Cavani and J. A. Odriozola, *ACS Catalysis*, 2018, **8**, 11154-11164.
4. Y. Wei, Y. Zhang, Y. Chen, F. Wang, Y. Cao, W. Guan and X. Li, *ChemSusChem*, 2022, **15**, e202101983.
5. L. Gao, K. Deng, J. Zheng, B. Liu and Z. Zhang, *Chemical Engineering Journal*, 2015, **270**, 444-449.
6. T. W. Chamberlain, V. Degirmenci and R. I. Walton, *ChemCatChem*, 2022, **14**, e202200135.
7. C. Fang, J.-J. Dai, H.-J. Xu, Q.-X. Guo and Y. Fu, *Chinese Chemical Letters*, 2015, **26**, 1265-1268.
8. M. El Fergani, N. Candu, M. Tudorache, P. Granger, V. I. Parvulescu and S. M. Coman, *Molecules*, 2020, **25**, 4885.
9. F. Yang, Y. Ding, J. Tang, S. Zhou, B. Wang and Y. Kong, *Molecular Catalysis*, 2017, **435**, 144-155.
10. F. Cheng, D. Guo, J. Lai, M. Long, W. Zhao, X. Liu and D. Yin, *Frontiers of Chemical Science and Engineering*, 2021, **15**, 960-968.
11. J. Lai, F. Cheng, S. Zhou, S. Wen, D. Guo, W. Zhao, X. Liu and D. Yin, *Applied Surface Science*, 2021, **565**, 150479.
12. F. Wang, J. Lai, Z. Liu, S. Wen and X. Liu, *Biomass Conversion and Biorefinery*, 2023, **13**, 16887-16898.
13. H.-z. LU, J.-f. BAI, Y. Fei, X.-y. ZHANG, J. Ying, J.-y. WANG, C. Ping and M.-d. ZHOU, *Journal of Fuel Chemistry and Technology*, 2021, **49**, 312-321.
14. A. B. Gawade, A. V. Nakhate and G. D. Yadav, *Catalysis Today*, 2018, **309**, 119-125.
15. S. Wang, Z. Zhang and B. Liu, *ACS Sustainable Chemistry & Engineering*, 2015, **3**, 406-412.
16. A. Tirsoaga, M. El Fergani, N. Nuns, P. Simon, P. Granger, V. I. Parvulescu and S. M. Coman, *Applied Catalysis B: Environmental*, 2020, **278**, 119309.
17. L.-S. Zhong, J.-S. Hu, A.-M. Cao, Q. Liu, W.-G. Song and L.-J. Wan, *Chemistry of Materials*, 2007, **19**, 1648-1655.
18. C. Yang, X. Yu, S. Heißler, A. Nefedov, S. Colussi, J. Llorca, A. Trovarelli, Y. Wang and C. Wöll, *Angewandte Chemie International Edition*, 2017, **56**, 375-379.
19. J. Holgado, G. Munuera, J. Espinós and A. González-Elipe, *Applied Surface Science*, 2000, **158**, 164-171.
20. P. Lokhande, K. Sonone and P. L. Dhepe, *New Journal of Chemistry*, 2023, **47**, 15325-15335.